Chapter 4

Improvement of the Quantum Dot-in-a-Well (QDWELL) Laser and Amplifier Performance under the Optical Injection

Yossef Ben Ezra and Boris I. Lembrikov

Additional information is available at the end of the chapter

http://dx.doi.org/10.5772/intechopen.69946

Abstract

Quantum dot (QD) laser devices can be successfully used in optical communications due to their unique properties caused by the carrier localization in three dimensions. In particular, quantum dot-in-a-well (QDWELL) lasers are characterized by an extremely low threshold current density and the high modulation frequency. However, their operation rate is limited by the strongly nonlinear electron and hole scattering rates in and out of QD. We investigated theoretically the nonlinear optical phenomena in QDWELL lasers and amplifiers under the optical injection. We have shown that the synchronization of the carrier dynamics in QD and quantum well (QW) caused by the optical injection improves the QDWELL laser performance and, in particular, enhances the relaxation oscillation (RO) frequency. As a result, the QDWELL laser performance in the analogous optical link (AOL) is significantly improving. The optical injection also improves the performance of the QDWELL-based semiconductor optical amplifiers (SOA).

Keywords: quantum dot (QD), quantum well (QW), laser, semiconductor optical amplifier (SOA), optical communications

1. Introduction

Advanced high-capacity communication systems are necessary for different applications, such as medical diagnosis, traffic safety, Internet, data services, etc. [1]. These new applications generate a giant data traffic which requires the time sensitive analysis and data processing at high-performance computing infrastructures (HPC) and the data storage, transport, and exchange in datacenters (DC) [1]. Recently, all-optical architecture of DC has been proposed.

It is based on the switching of all data in the optical domain [1]. This approach requires the development of new photonic devices [1]. One of the most efficient technologies for the realization of such devices is Silicon Photonics. Silicon Photonics can resolve the so-called bandwidth bottleneck by the integration of photonic integrated circuits (PIC) and electronic integrated circuits [1]. The active components such as lasers are made of the III-V compositions. There are two techniques of the III-V laser integration with PIC: (i) the III-V laser die can be butt-coupled to the silicon photonic chip using active alignment and (ii) III-V materials are wafer bonded to the silicon photonic chip in order to fabricate lasers lithographically aligned to the silicon waveguide circuit [1].

A generic optical communication system consists of an optical transmitter, optical communication channel, and an optical receiver [2]. A block diagram of such a system is shown in **Figure 1** [2].

The information highways providing these services are based on optical fibers [1]. Typically, silica optical fibers are used as the communication channel due to their low losses of about 0.2 dB/km [2]. In such a case, the losses are 20 dB after the propagation distance of 100 km, and the optical power decrease by 100 times defines the amplifier spacing in the long-haul lightwave systems [2, 3]. In long-haul networks extended over thousands of kilometers fiber losses are compensated by using a chain of amplifiers boosting the signal power periodically to its original value [1, 2]. Erbium-doped fiber amplifiers (EDFA) are widely used in optical communication systems due to their compatibility with transmission fibers, energy efficiency, and low cost [1, 2]. Raman amplifier operation is based on the stimulated Raman scattering (SRS) in silica fibers [2]. The advantages of the Raman amplifiers are the using of the fiber itself as an active medium and the large bandwidth [2]. However, the Raman amplifiers require a comparatively large pumping power [2].

The optical communication system performance is limited by the fiber dispersion leading to the optical pulse broadening with propagation through the channel [2, 3]. As a result, the original signal recovery with the high enough accuracy may be impossible [2]. The dispersion influence is strongly manifested in multimode fibers (MMFs) where different fiber modes propagate with different velocities. For this reason, optical communication systems are mainly based on single-mode fibers (SMFs) [2]. In such a case, the intermodal dispersion vanishes because the pulse energy is carried by a single mode [2]. The main types of the SMF dispersion are as follows: (i) group velocity dispersion (GVD) is caused by group velocity v_g frequency dependence (chromatic dispersion); (ii) material dispersion is caused by the silica refractive index n dependence on the optical frequency; (iii) waveguide dispersion is defined by the following parameters: the fiber

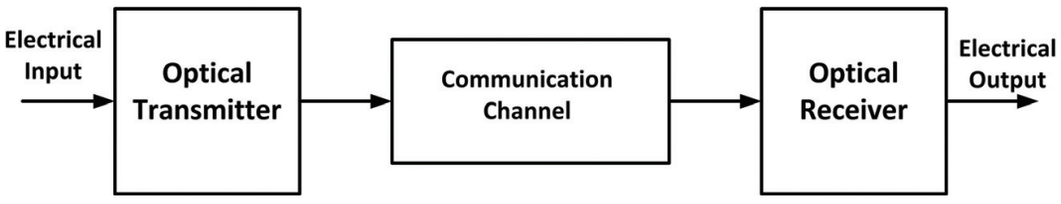

Figure 1. A block diagram of a generic optical communication system.

core radius r_0, the fiber core refractive index n_1 and the cladding refractive index n_2; and (iv) polarization-mode dispersion (PMD) is caused by a modal birefringence [2, 3]. SMF material dispersion is small enough, and it actually limits the optical communication system bit rate and transmission distance under the condition that other types of dispersion are mitigated [2].

Optical transmitter converts the electrical signal into the optical signal and launches it into the optical fiber [2]. An optical transmitter consists of an optical source, a modulator, and a channel coupler [2]. An optical source is usually a semiconductor laser or light-emitting diode (LED) compatible with the optical communication channel [2]. In LED, population inversion is not realized, and the light is generated through spontaneous emission caused by the radiative recombination of electron-hole pairs in the active layer [2]. In semiconductor lasers, the stimulated emission of light is the dominating operation mechanism [2, 4]. For this reason, the LED radiation is rather weak as compared to the semiconductor laser light. The typical values of the launched power are less than 100 μW (−10 dBm) for LED and about 1 mW (10 dBm) for semiconductor lasers [2]. The optical signal is generated by the direct or external modulation of the optical carrier wave radiated by a semiconductor laser [2]. Generally, time, quadrature, polarization, and frequency are widely used in optical networking technologies for complex quadrature modulation formats, polarization multiplexing, digital pulse shaping, and coherent detection [1]. Recently, space as a physical dimension for modulation and multiplexing in communication systems attracted interest for fiber capacity scaling [1]. Space-division multiplexing (SDM) uses multiplicity of space channels, or spatial parallelism, in order to increase capacity of the optical communication system [1]. For instance, fiber bundles 10×10 Gb/s or 4×25 Gb/s can be used for the implementation of 100 Gb/s commercial client interfaces [1].

In the case of the direct modulation, the semiconductor laser is biased near the threshold and driven by the electrical sinusoidal signal for analog modulation or electrical signal bit stream for digital modulation [2]. In the case of the external modulation, two types of the external modulators are mainly used: the Mach-Zehnder modulator (MZM) and the electro absorption modulator (EAM) [2, 4]. The channel coupler is a microlens focusing the optical signal onto the optical fiber entrance plane [2]. The bit rate of optical transmitters is limited by electronic components [2].

An optical receiver converts the optical signal into the electrical domain and recovers the transmitted data [2, 4]. The structure of the optical receiver depends on the modulation format. Consider first the on-off keying (OOK) modulation, where an electrical binary stream modulates the optical carrier intensity inside an optical transmitter [2, 4]. In such a case, the directly modulated optical signal after the propagation through the optical fiber is converted in the receiver directly into the original digital signal in the electrical domain [2]. The main component of the receiver is a semiconductor photodetector (PD) converting light into electrical signal through the photoelectric effect [2]. Such a communication system is intensity modulation with direct detection (IM/DD) system [2]. PD should possess high sensitivity, fast response, low noise, low cost, and high reliability [2]. Generally, the transmission quality is characterized by the received signal-to-noise ratio (SNR) given by $SNR = 20log_{10}(A_{max}/A_N)$ dB, where A_{max} and A_N are the maximum amplitude of the given analog signal and the root mean square (RMS) noise amplitude of the analog signal, respectively [2]. The total noise is a stochastic process consisting of a number of components such as mode partition noise (MSN),

laser intensity noise, modal noise, shot noise, thermal noise, dark current noise, amplified spontaneous emission (ASE), and crosstalk noise [4]. The shot noise and thermal noise are the two fundamental noise mechanisms responsible for the current fluctuations in optical receivers [2]. The detailed analysis of the different types of noise may be found in Refs. [2–4]. Here, we should note that the thermal noise limits PD performance in practice, whereas the shot noise determines a fundamental limit of PD operation [2]. For instance, in the shot-noise limit, SNR = 20 dB can be realized for PD quantum efficiency close to unity and a number of photons $N_p = 100$ in the input optical signal [2].

Unlike the IM/DD system, the performance of the system with a coherent detection technique is limited by the shot-noise alone [2, 4, 5]. Another important advantage of the coherent detection is the possibility of the detection of signals with advanced modulated formats such as frequency-shift keying (FSK), binary phase-shift keying (PSK), quadrature PSK, and 16-quadrature amplitude modulation (QAM) allowing bit rates of 50, 100, and 200 Gb/s [1, 2, 4]. In the case of the coherent detection, the input optical signal with the optical carrier frequency ω_0 is mixed with the continuous wave (CW) optical signal generated at the receiver by a narrow linewidth laser called the local oscillator (LO) with the frequency ω_{LO} [2]. The output contains the signal with the intermediate frequency $\omega_{IF} = \omega_0 - \omega_{LO} \ll \omega_0$ which falls on PD [2]. There are two types of the coherent detection technique: (i) a homodyne detection when $\omega_0 = \omega_{LO}; \omega_{IF} = 0$; (ii) a heterodyne detection when $\omega_0 \neq \omega_{LO}$ [2, 4]. In the latter case, the detection of the optical signal is carried out in two stages: first, the carrier frequency ω_0 is converted to the intermediate frequency ω_{IF} usually belonging to the radio frequency (RF) range; then, the RF signal is down converted to the modulating signal bit stream [2, 4].

Optical signal processing in optical communication systems is based on the linear and nonlinear optical techniques used for the manipulation and processing of digital, analogue, and quantum information [1]. Ultrafast optical nonlinearities provide an operation rate advantage as compared to the electronic techniques for switching, regeneration, wavelength conversion, performance monitoring, and analog digital conversion (ADC) [1]. In particular, semiconductor optical amplifiers (SOAs) can be used in such applications due to their high operation rate and strong nonlinearity [1–3].

The brief review of the optical communication systems clearly shows that a semiconductor laser is a key component of both the transmitter and receiver. Evidently, for the highly efficient applications in optical communication systems, semiconductor laser performance should be characterized by low-threshold current, high-speed direct modulation, ultrashort optical pulse generation, narrow spectral linewidth, broad modulation bandwidth, comparatively high optical output power, low relative intensity noise (RIN), low cost, and low electrical power consumption [2, 6]. The objective of this chapter is the investigation of the optical injection influence on the performance of the novel semiconductor laser based on quantum dots (QD) in a quantum well (QW) structure. The number of publications concerning semiconductor lasers in general and QD lasers in particular is enormous and hardly observable. For this reason, in Section 2, we briefly discuss the structure, operation principle, and basic characteristics of a semiconductor laser widely used in optical communication systems. In Section 3, the fundamentals of a QD in QW (QDWELL) laser and SOA are discussed. The original theoretical

http://dx.doi.org/10.5772/intechopen.69946

results related to the dynamics and performance of the optically injected QDWELL lasers and SOA are presented in Section 4. The conclusions are presented in Section 5.

2. Structure and operation principle of a semiconductor laser

Semiconductor laser is an electrically pumped p-i-n diode [6]. In the forward-biased diode, electrons in the conduction band and holes in the valence band are injected into the active layer placed between the p-type and n-type cladding layers [2, 6]. The structure of an edge-emitting semiconductor laser is shown schematically in **Figure 2** [2].

The cladding layers are made of the semiconductor material with the bandgap E_{g2} larger than the active layer bandgap E_{g1} [2, 6]. Such a structure consisting of the p-n junctions made of semiconductor materials with different bandgaps is called a heterostructure [2, 7]. As a result, the electrons and holes are confined in the active layer.

The $Al_xGa_{1-x}As/GaAs/Al_xGa_{1-x}As$ heterostructure is shown in **Figure 3** [6]. The concentration of donors N_D and acceptors N_A in the n-type and p-type regions, respectively, should satisfy the condition that the separation $E_{FC} - E_{FV}$ between the electron Fermi energy level E_{FC} and the hole Fermi energy level E_{FV} is larger than the bandgap energy E_g [2]. Recombination of the electron-hole pair in the presence of the optical field results in the photon stimulated emission [2, 6].

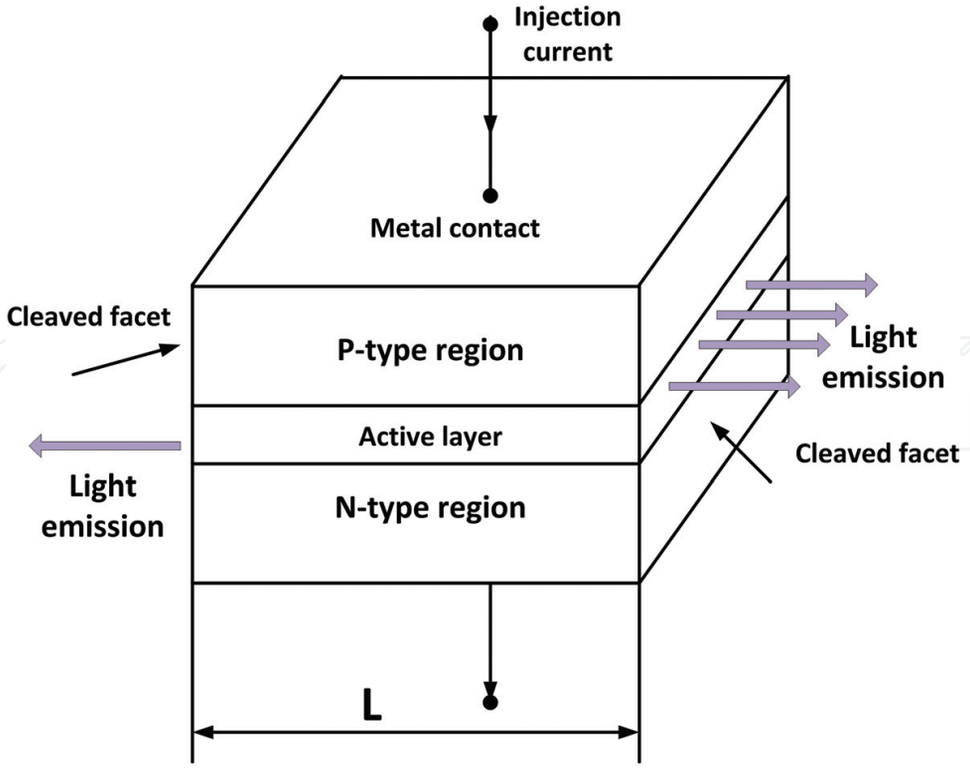

Figure 2. Edge-emitting semiconductor laser.

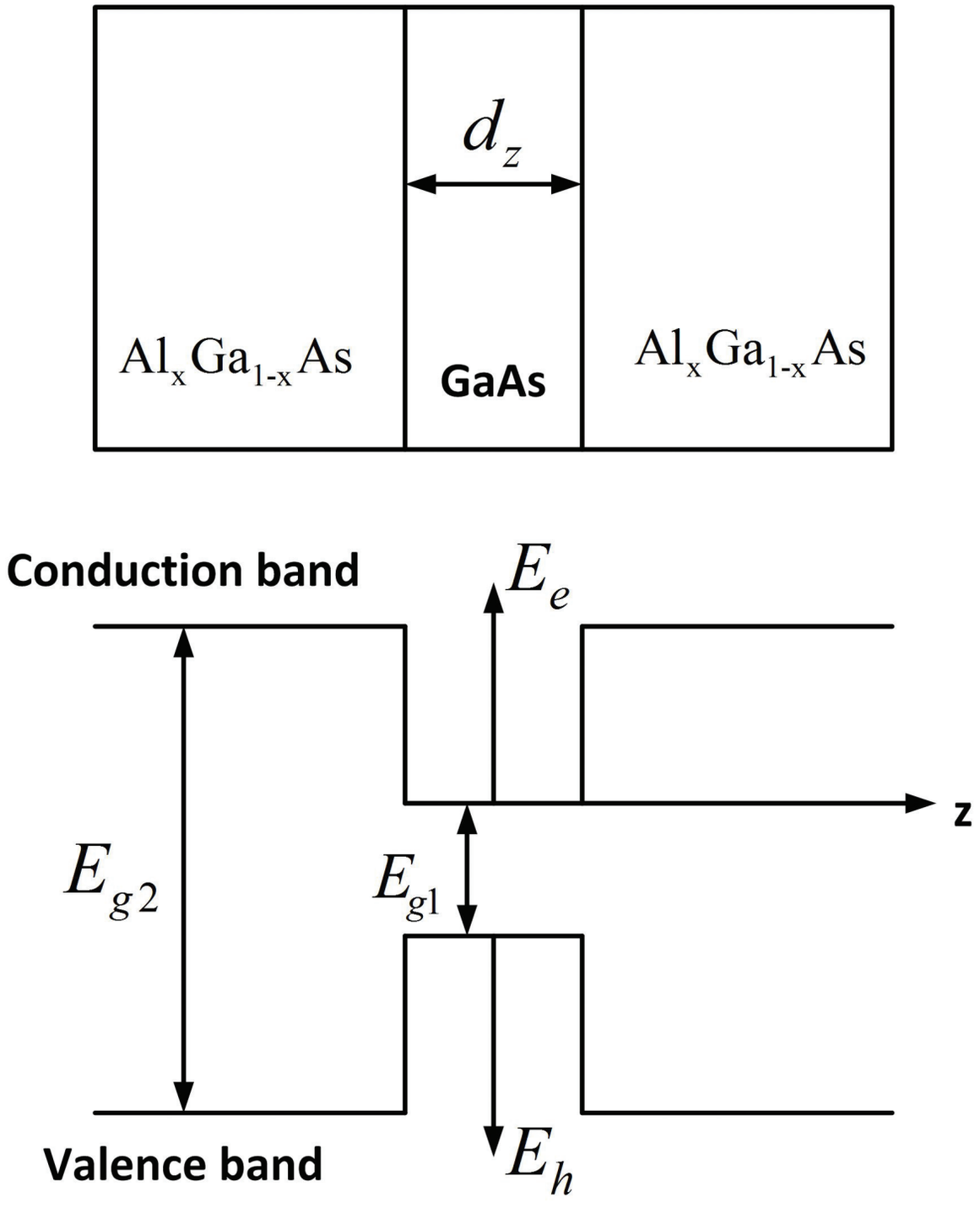

Figure 3. The energy bands of the semiconductor laser based on the $Al_xGa_{1-x}As/GaAs/Al_xGa_{1-x}As$ heterostructure.

Usually, the active layer has a larger refractive index than the cladding layers providing also the confinement of the photons generated in the active layer [2]. When the injected carrier density in the active layer becomes larger than a critical value, the population inversion occurs and the active region manifests an optical gain [2]. Input signal intensity P_{in} in such a case is amplified, and the output signal intensity P_{out} has the form [2]

$$P_{out}(L) = P_{in}(0)\exp(gL) \tag{1}$$

where g is the power gain coefficient and L is the active layer length. Usually, the laser dimensions are less than 1 mm in all three directions which result in compact design [2]. The gain is negative $g < 0$ for the injected carrier density N below the population inversion value. The gain becomes positive and increases with the increase of the injected carrier density N. The peak gain g_p is given by the approximate empirical relationship [2].

$$g_p(N) = \sigma_g(N - N_T) \tag{2}$$

where σ_g is the gain cross section or the differential gain and N_T is the transparency value of the carrier density. For InGaAsP lasers, the typical values of these parameters are following: $\sigma_g \approx (2-3)\times 10^{-16}$ cm^{-2}, $N_T \approx (1-1.5)\times 10^{18}$ cm^{-3} [2]. Eq. (2) can be used in the high-gain region where g_p >100 cm^{-1} [2]. The laser operation also requires an optical feedback provided by placing the gain medium into a Fabry-Perot (FP) cavity formed in our case by the two cleaved laser facets serving as mirrors [2]. In such a case, a critical value of the gain g_{cr} is given by [2]

$$g_{cr} = \alpha_{\text{int}} + \frac{1}{2L}\ln\left(\frac{1}{R_1R_2}\right) \tag{3}$$

where α_{int} is the coefficient of the internal losses caused by free carrier absorption and interface scattering and $R_{1,2}$ are the facet reflectivities. In the laser FP cavity, only the longitudinal modes can exist determined by the condition [2]

$$2\beta L = m\pi;\ \beta = \frac{2\pi\nu n_{\text{mode}}}{c};\ \nu = \nu_m = \frac{mc}{2n_{\text{mode}}L};\ m = 1, 2, \ldots \tag{4}$$

where β, n_{mode}, and c are the mode propagation constant, the mode refractive index, and the free space light velocity, respectively. Eq. (4) shows that the laser frequency ν corresponds to the discrete spectrum of the laser longitudinal modes. A semiconductor laser radiation typically consists of several longitudinal modes with a gain spectrum bandwidth of about 10 THz [2]. The dominant mode is the one with gain closest to the peak gain g_p [2]. The optical modes penetrate into the cladding layers due to the boundary conditions for the optical mode electric and magnetic field while the gain takes place only in the active layer. Hence, the confinement factor of the active layer $\Gamma = g/g_m$ is introduced which is typically less than 0.4 [2]. Here, g_m is the so-called material gain. The modes propagate inside the optical fiber with different speeds because of GVD as it was mentioned above. Consequently, the multimode semiconductor lasers are limiting the optical communication operation rate [2].

There exist single-mode semiconductor lasers emitting light mainly in a single longitudinal mode such as distributed feedback (DFB) lasers, coupled-cavity lasers, tunable lasers, and vertical-cavity surface-emitting lasers (VCSEL) [2]. The detailed analysis of structure and operation principles of these lasers can be found in Ref. [2] and references therein. Here, we

only briefly discuss the peculiarities of these lasers following Ref. [2]. DFB laser has a built-in periodic grating with the period d_0 which results in refraction index periodicity. Consequently, the waves propagating in the forward and backward directions in the cavity are coupling, and the Bragg diffraction occurs. The feedback in such a case is distributed throughout the laser cavity length. The coupling occurs only for the modes with the Bragg wavelength λ_B satisfying the Bragg condition $d_0 = (\lambda_B/2n_{\text{mode}})m$, $m = 1, 2, 3, \ldots$ [2]. This condition provides the mode selectivity of the DFB lasers. The strongest coupling between the forward and backward propagating modes occurs for $m = 1$ [2].

In a coupled-cavity semiconductor laser, single-mode operation is realized by coupling the laser cavity to an external cavity. The in-phase feedback occurs only for the laser modes with a wavelength which almost coincides with a certain longitudinal mode of the external cavity [2]. The effective reflectivity of the laser facet close to the external cavity depends on the wavelength, and the losses of certain modes sharply decrease. The longitudinal mode which simultaneously has the highest gain and the lowest cavity loss becomes the dominant mode [2].

A tunable semiconductor laser typically consists of three sections: the active section, the phase-control section, and the Bragg section [2]. Each one of these sections is biased independently by injecting different currents in a following way: the current injected into the Bragg section changes the Bragg wavelength λ_B through carrier induced variations in the refractive index n; the current injected into the phase-control section changes the feedback phase through carrier induced variations in the refractive index of this section [2]. As a result, the laser wavelength can be tuned over the range of 10–15 nm by controlling the injection current in the phase-control and the Bragg sections [2].

VCSEL emits light in a direction perpendicular to the active layer plane and operates in a single longitudinal mode regime due to the small cavity length of about 1 μm in a wide range of wavelengths of about 650–1600 nm [2]. The emitted light has a form of a circular beam which can be inserted into SMF with high efficiency [2].

The dynamics of the single-mode semiconductor laser is described by the following rate equations for the number of electrons N and photons P in the active layer [2].

$$\frac{dP}{dt} = GP + R_{sp} - \frac{P}{\tau_p} \tag{5}$$

$$\frac{dN}{dt} = \frac{I}{q} - \frac{N}{\tau_c} + GP \tag{6}$$

where I is the injection current, q is the electron charge, $G = \left(\Gamma v_g \sigma_g / V\right)(N - N_0)$ is net rate of the stimulated emission, V is the active layer volume, $N_0 = N_T V$, v_g is the light group velocity, R_{sp} is the spontaneous emission rate, and τ_p are τ_c are the photon and carrier lifetime, respectively. The threshold current I_{th} for the laser generation regime obtained from the steady-state solution of Eqs. (5) and (6) has the form [2].

$$I_{th} = \frac{q}{\tau_c}\left(N_0 + \frac{V}{G_N \tau_p}\right); \qquad G_N = \frac{\Gamma v_g \sigma_g}{V} \tag{7}$$

The direct modulation of the laser emission can be realized if the injection current includes a time-dependent component. In the case of a sinusoidal modulation, the modulation frequency ω_m is limited by the relaxation oscillation (RO) frequency Ω_R given by [2]

$$\Omega_R = \left[GG_N P_b - \frac{\left(\Gamma_P - \Gamma_N\right)^2}{4} \right]^{1/2} \tag{8}$$

where P_b is the steady-state photon number, $\Gamma_P = \left(R_{sp}/P_b\right) + \varepsilon_{NL} G P_b; \Gamma_N = \tau_c^{-1} + G_N P_b$, ε_{NL} is a nonlinear gain parameter, and $\Gamma_R = (\Gamma_N + \Gamma_P)/2$ is a damping rate of the relaxation oscillations. The efficiency of the laser modulation is significantly reduced for $\omega_m > \Omega_R$ [2]. The 3 dB modulation bandwidth f_{3dB} of the semiconductor laser is also determined by the RO frequency Ω_R. For $\Omega_R \gg \Gamma_R$, it has the form $f_{3dB} \approx \left(\sqrt{3}\Omega_R\right)/2\pi$ [2].

Consider now QW semiconductor lasers based on a heterostructure shown in **Figure 3**. If the thickness of the active layer d_z is less than approximately 10 nm, the confined electrons and holes exhibit quantum effects, and such a heterostructure is called a single QW [6, 7]. In such a case, the De Broglie electron wavelength $\lambda = h/p$ in a semiconductor is close to the active layer thickness [7]. Here, h, p are the Planck constant and electron momentum, respectively. The charge carriers in a QW laser are localized in the z direction perpendicular to the active layer plane and represent a two-dimensional (2D) electron and hole gas [6]. The solution of the Schrödinger equation for carriers in QW produces discrete states of energy E_n in the z direction perpendicular to the QW plane and a continuous range of allowed energies in the QW plane [7]. The electron energy E_e in a QW is given by [6, 7]

$$E_e = E_n + \frac{\hbar^2\left(k_x^2 + k_y^2\right)}{2m_e^*} \tag{9}$$

where $\hbar = h/2\pi$, m_e^* is the electron effective mass, and $k_{x,y}$ are the electron continuous momentum components in the QW plane [6, 7]. Similar expression can be written for the hole energy in QW. The threshold current in a 2D structure reduces significantly as compared to the bulk semiconductor laser [6]. The electronic and optical properties of a semiconductor laser strongly depend on the carrier density of states (DOS) $\rho_{e,h}(E_{e,h})$.The electron DOS in a QW with n_e energy levels has the form [6, 7]

$$\rho_e(E_e) = \sum_{n_e} \frac{m_e^*}{\pi\hbar^2} u(E_e - E_n); u(x) = \begin{cases} 1, x > 0 \\ 0, x < 0 \end{cases} \tag{10}$$

Similar expression can be written for the hole DOS. It is seen from Eq. (10) that carrier DOS in QW does not depend on the energy. The static and dynamic properties of the QW semiconductor laser can be described by the rate equations for the carrier density in QW N_W and in a separate confinement heterostructure (SCH) layer N_B, and the photon density in the cavity P given by [8]

$$\frac{dN_B}{dt} = \frac{I}{qV_{SCH}} - \frac{N_B}{\tau_r} - \frac{N_B}{\tau_{nb}} + \frac{N_W V_W}{\tau_e V_{SCH}} \tag{11}$$

$$\frac{dN_W}{dt} = \frac{N_B V_{SCH}}{\tau_r V_W} - \frac{N_W}{\tau_n} - \frac{N_W}{\tau_{nr}} - \frac{N_W}{\tau_e} - \frac{v_g G(N_W) P}{1 + \varepsilon P} \tag{12}$$

$$\frac{dP}{dt} = \frac{\Gamma v_g G(N_W) P}{1 + \varepsilon P} - \frac{P}{\tau_p} + \Gamma \beta_{Sp} \frac{N_W}{\tau_n} \tag{13}$$

where τ_n, τ_{nr}, τ_{nb}, τ_r, and τ_e are the radiative recombination lifetime in QW, the nonradiative recombination lifetime in QW, the total recombination lifetime in the SCH region, the carrier transport time across the SCH to QW active region, and the carrier thermionic emission time from QW into the barrier and SCH layers, respectively; β_{Sp} is the spontaneous emission feedback factor, $G(N_W)$ is the carrier density dependent gain, ε is the intrinsic gain compression factor, and V_W and V_{SCH} are the QW and SCH volumes, respectively. The rate equations for QW laser (11)–(13) are different from the bulk laser Eqs. (5) and (6). The additional Eq. (11) includes the effects of the carrier transport in SCH region typically used in QW lasers for the carrier and optical confinement [6, 8].

3. Structure and theoretical model of a quantum dot-in-a-well (QDWELL) laser and SOA

QD is a nanostructure where the electron and hole motion is confined in three dimensions reducing the degrees of freedom to zero [7, 9]. The III-V QDs are grown epitaxially on a semiconductor substrate [9]. The spontaneous formation of 3D islands during strained layer epitaxial growth is known as the Stranski-Krastanov process [9]. A continuous film of a QW thickness beneath the QD is called the wetting layer (WL) [9, 10]. In QD, carriers occupy a finite number of energy levels defined by the solution of the Schrödinger equation for a 3D potential separating the inside of QD from the outside [7]. Typically, the spherical and pyramidal QD models are used [7]. The pyramidal model is more realistic since the QD grown by means of the Stranski-Krastanov technology have approximately pyramidal form [9]. In such a case, the Schrödinger equation for QD can be solved numerically [7, 9]. Carrier DOS in QD is a $\delta-$ function for each energy level [7]. QD has a lateral size of approximately 15–18 nm, a height of about 4–5 nm, and contains several hundreds of thousands of atoms [9, 10]. The QD density per unit area in each layer is about $10^{10} - 10^{11}$ cm^{-2} [9, 10]. QD lasers exhibit extremely low threshold current due to the 3D carrier confinement [9, 10]. The spectral bandwidth of QD lasers is broader than the one of the QW lasers due to the inhomogeneous spectral broadening caused by QD size variations that exhibit a Gaussian size distribution and consequently a nearly Gaussian distribution of the emitted light frequencies [9]. Semiconductor lasers based on self-organized InGaN, InAs, InGaAlP, and In(Ga)As QD are promising candidates for applications in optical communication systems because of their low threshold current, high temperature stability, fast carrier dynamics, and the possibility of the light emission from ultraviolet to the far infrared spectral regime [9–13]. Typically, the active area of a QDWELL

http://dx.doi.org/10.5772/intechopen.69946

laser consists of several QW layers each one of a height of 4 nm with the embedded 3D confined QD having an average size of approximately 4 nm × 18 nm × 18 nm [10]. An electric current is injected into the QW layers which form the carrier reservoir (WL) where the carrier-carrier scattering leads to a filling or depletion of the confined QD levels [10]. The energy band structure of a QDWELL laser is shown in **Figure 4**. Inside the QD, the lower level or the ground state (GS) and several higher levels or excited states (ES) for electrons and holes may exist [11]. We discuss the QDWELL laser model with the GS and one ES where the emission occurs form GS [10]. In QDWELL lasers, the Coulomb interaction is the essential mechanism of the carrier-carrier scattering for high carrier densities in WL [10].

The turn-on dynamics, the small signal and large signal responses of a QDWELL laser have been studied theoretically and experimentally in the fundamental works of Lüdge, Schöll and co-workers [10, 13–18].

It has been shown that the complicated carrier dynamics in a QDWELL laser is determined by the nonradiative carrier-carrier scattering processes between the QD and the QW [17]. The

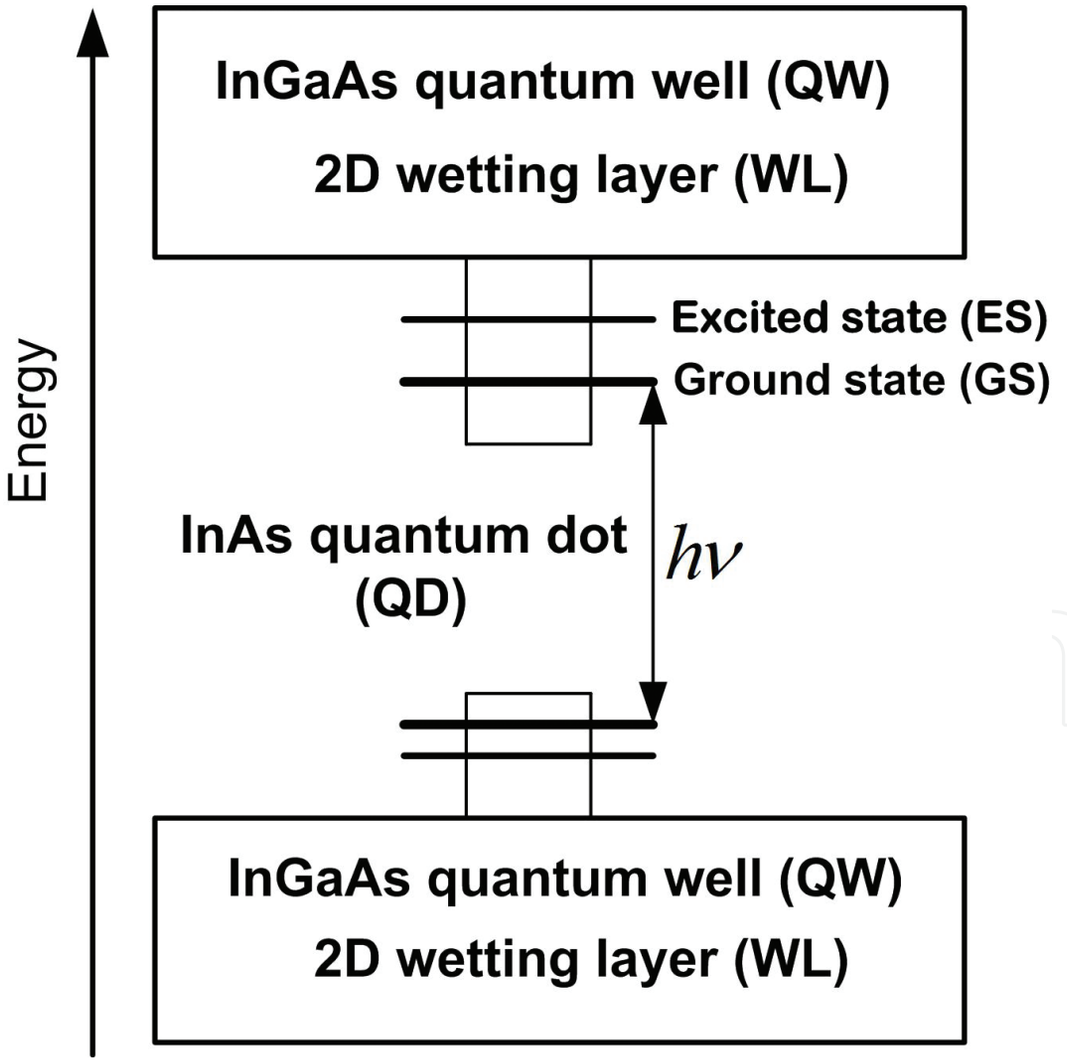

Figure 4. The energy band structure of a QDWELL laser.

corresponding scattering rates S_e^{in}, S_e^{out}, S_h^{in}, S_h^{out} of electrons (e) and holes (h) for scattering in and out of the QD are strongly nonlinear and depend on the electron and hole occupation probabilities in the confined QD levels ρ_e, ρ_h and the electron and hole densities in the QW w_e, w_h [13–18]. The electron and hole scattering times are given by, respectively, $\tau_e = \left(S_e^{in} + S_e^{out}\right)^{-1}$ and $\tau_h = \left(S_h^{in} + S_h^{out}\right)^{-1}$ [14, 16, 18]. The carrier relaxation processes in QD states are much faster than the capture processes from the QW into the QD at high carrier densities in the QW WL, and the influence of the higher QD levels can be adiabatically eliminated [17].

The nonlinearity of the scattering rates S_e^{in}, S_e^{out}, S_h^{in}, S_h^{out} and the separate dynamics of holes and electrons are essential for the QDWELL laser dynamics adequate description [16]. The electron and hole dynamics in the QDWELL laser is desynchronized due to different effective masses and different energy separation between 2D WL band edge and confined QD level [16]. The QD hole density is changing more slowly as compared to the electron density [16]. Desynchronized carrier dynamics results in the deterioration of the laser performance both in the small-signal and in the large-signal regimes [15, 17]. In particular, the QDWELL laser modulation frequency is limited by the RO frequency of 7 GHz [17]. The relatively slow carrier scattering processes from 2D WL carrier reservoir into confined QD levels are responsible for the high damping of the turn-on process and the flat modulation response curve of QDWELL lasers [10]. Usually, the modulation frequency can be increased by increasing the injection current, but in our case, the injection current increase results in the device heating and the further reduction of the RO frequency [17].

The modulation characteristics of semiconductor lasers can be improved by the optical injection locking (OIL) [19]. OIL of semiconductor lasers provides a single-mode regime and near-single-sideband modulation, strongly enhances the RO frequency and bandwidth, reduces nonlinearity, reduces RIN, reduces chirp, and increases link gain [19]. The directly modulated OIL transmission-style system combining the master laser and the slave QDWELL laser in the transmission style is shown in **Figure 5** [19].

In the transmission-style system, the injected light from the master laser enters one slave QDWELL laser facet and output is taken from the other facet [19]. The direct modulation signal is applied to the QDWELL slave laser. An isolator prevents light coupling back to the master laser. A polarization controller (PC) is used to match the overlap of master and QDWELL slave laser polarizations. The master laser light coherently combines with the QDWELL slave laser

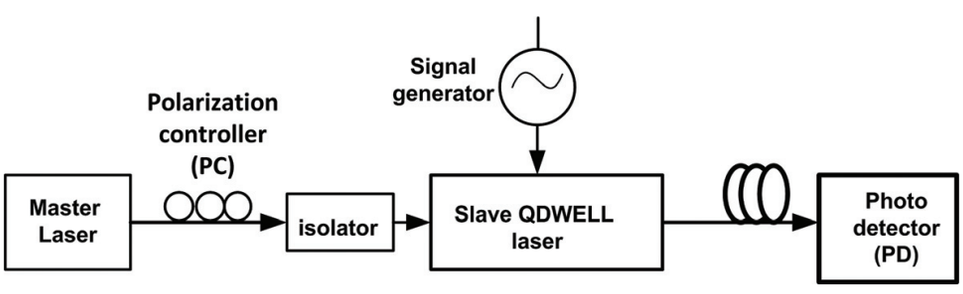

Figure 5. Directly modulated OIL system.

light changing its internal field [19]. The slave laser radiation wavelength tends to the master laser radiation wavelength until the both wavelengths become equal locking the master laser light frequency and phase [19].

The dynamics of the optically injected QDWELL laser has been studied theoretically by using the Lüdge-Schöll (LS) rate equations for the photon density per unit area n_{ph} and the phase Φ of the slave QDWELL laser radiation, the QD electron and hole occupation probabilities ρ_e, ρ_h, and the electron and hole densities in the QW w_e, w_h [20].

$$\frac{dn_{ph}}{dt} = n_{ph}\left[2\tilde{W}Z_a^{QD}\left(\rho_e + \rho_h - 1\right) - 2\kappa\right] + \frac{\beta_{Sp}}{A}2Z_a^{QD}R_{sp}\left(\rho_e, \rho_h\right) + \frac{2K}{\tau_{in}}\sqrt{n_{ph}n_{ph}^0}\cos\left(\Phi - 2\pi\Delta\nu_{inj}t\right) \tag{14}$$

$$\frac{d\Phi}{dt} = \frac{\alpha}{2}\left[2\tilde{W}\left(\rho_e + \rho_h - 1\right) - 2\kappa\right] + \frac{2K}{\tau_{in}}\sqrt{\frac{n_{ph}^0}{n_{ph}}}\sin\left(\Phi - 2\pi\Delta\nu_{inj}t\right) \tag{15}$$

$$\frac{d\rho_{e,h}}{dt} = -\tilde{W}A\left(\rho_e + \rho_h - 1\right)n_{ph} - R_{sp}\left(\rho_e, \rho_h\right) + S_{e,h}^{in}(w_e, w_h)\left(1 - \rho_{e,h}\right) - S_{e,h}^{out}(w_e, w_h)\rho_{e,h} \tag{16}$$

$$\frac{dw_{e,h}}{dt} = \frac{j}{q} - 2N^{QD}\left[S_{e,h}^{in}(w_e, w_h)\left(1 - \rho_{e,h}\right) - S_{e,h}^{out}(w_e, w_h)\rho_{e,h}\right] - \tilde{R}_{sp} \tag{17}$$

Here, A is the in-plane area of the QW, ν_L and ν_{inj} are the close frequencies of the QDWELL laser and the injected light, respectively, $K = \sqrt{T_{inj}n_{inj}/n_{ph}^0}$ is the injection strength, T_{inj} is the transmission coefficient of the cavity mirror, n_{inj} is the injected photon density in the QDWELL laser active region, and n_{ph}^0 is the steady-state photon density without injection; $\Delta\nu_{inj} = \nu_{inj} - \nu_L$ is the input detuning, $Z_a^{QD} = a_L A N_a^{QD}$ is the number of active QDs inside the waveguide, a_L is a number of self-organized QD layers, N_a^{QD} is the density per unit area of the active QD of a lasing subgroup, N^{QD} is the density per unit area of all QDs; 2κ are the optical intensity losses; $\tilde{W}$, and W are the Einstein coefficients for the coherent and incoherent interaction of the QD with all resonator modes, respectively; α is the linewidth enhancement factor (LEF), β_{Sp} is the spontaneous emission factor, $R_{sp}\left(\rho_e, \rho_h\right)$, and $\tilde{R}_{sp}$ are the spontaneous emission rates in QD and QW, respectively; τ_{in} is the time of one round trip of the light in the cavity of length L. We do not present here the complicated explicit expressions of the scattering rates S_e^{in}, S_e^{out}, S_h^{in}, S_h^{out} which can be found in Ref. [20]. It has been shown that the QDWELL laser's dynamic properties under optical injection are strongly influenced by the Coulomb scattering processes which can be taken into account by using the microscopically calculated carrier lifetimes $\tau_{e,h}$ [20]. The nonlinear dynamics of the optically injected QDWELL laser is determined by the injection strength and the input detuning [20]. The frequency-locking range depends on the pump current. The photon density as well as the electron and hole densities in QD and QW increase with increasing the pump current which results in the change of scattering rates and the QDWELL turn-on behavior [20]. The QDWELL laser under the optical injection manifests complex oscillatory dynamics for a comparatively large detuning $\Delta\nu_{inj}$ [20]. The large regions

of stable CW operation occur for the short carrier lifetimes of about 10 ps typical for strongly damped relaxation oscillations [20].

Under certain conditions, QDWELL laser can operate as a SOA for high-speed applications [9]. Generally, SOA is the LED amplifying the input optical signal. SOAs are divided into two groups depending on their structure: (i) traveling wave amplifiers (TWA) and (ii) FP cavity amplifiers [9]. The block diagram of the TWA QDWELL SOA is shown in **Figure 6**.

SOA attracted a wide interest for applications in optical communication systems due to their small size, high gain, strong nonlinearity, and the possibility of on-chip optoelectronic integration [2, 9]. QD SOAs are particularly promising candidates for the amplification of ultrafast pulses in the relatively broad spectral range due to their ultrafast carrier dynamics and inhomogeneous spectral broadening [9]. The SOA dynamics is described by the carrier rate equations, equation for the time-dependent SOA gain and the equations for the slowly varying envelopes (SVE) of the optical pulses [2, 9].

The system of rate equations (14)–(16) should be modified for the case of a TWA QDWELL SOA. Eq. (17) for the electron and hole densities in the QW w_e, w_h does not change. The modified equations for the pumping and signal photon densities per unit area $n_{ph,p,s}$, phases $\Phi_{p,s}$, and the QD electron and hole occupation probabilities ρ_e, ρ_h in QDWELL SOA have the form [20–23].

$$\frac{\partial n_{ph,p,s}(z,\tau)}{\partial z} = \left(g_{\text{mod } p,s} - 2\kappa\right) n_{ph,p,s}(z,\tau) \tag{18a}$$

$$\frac{\partial \Phi_{p,s}}{\partial z} = -\frac{\alpha}{2} g_{\text{mod } p,s} \tag{18b}$$

$$\frac{d\rho_{e,h}}{dt} = -\tilde{W}A\left(\rho_e + \rho_h - 1\right)\left(n_{ph,p} + n_{ph,s}\right) - R_{sp}\left(\rho_e, \rho_h\right) + S^{in}_{e,h}(w_e, w_h)\left(1 - \rho_{e,h}\right) - S^{out}_{e,h}(w_e, w_h)\rho_{e,h} \tag{19}$$

where $\tau = t - z/v_g$, and $g_{modp,s}$ is the modal gain [22].

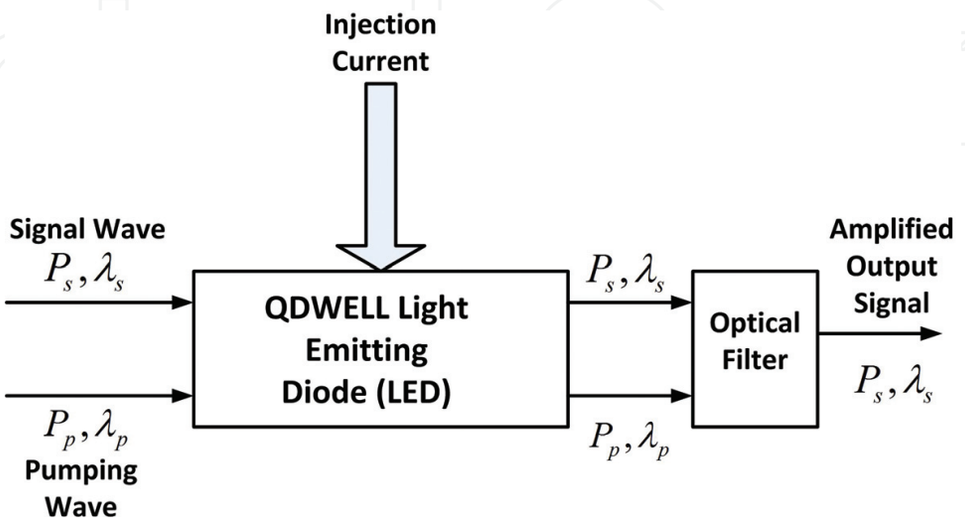

Figure 6. The block diagram of TWA QDWELL SOA.

$$g_{\mathrm{mod}} = \frac{2\Gamma}{r_{QD}} N^{QD} \int d\omega_i F(\omega_i)\sigma_i(\omega_0)\left(\rho_e + \rho_h - 1\right) \tag{20}$$

Here, r_{QD} is the mean size of QD, $\sigma_i(\omega_0)$ is the cross section of interaction of photons of frequency ω_0 with carriers in QD at the transition frequency ω_i:

$$\sigma_i(\omega_0) = \frac{\sigma_{res}}{1 + (\omega_i - \omega_0)^2 T_2^2} \tag{21}$$

where σ_{res} is the resonant cross section, $T_2 = 2\gamma_{hom}^{-1}$ is the dephasing time, and γ_{hom} is the homogeneous full width of half maximum (FWHM). The distribution function $F(\omega_i)$ of the transition frequency in the QD ensemble describes the inhomogeneous broadening caused by the QD size variation. It is assumed to be Gaussian and has the form [22]

$$F(\omega_i) = \frac{1}{\Delta\omega\sqrt{\pi}} \exp\left[-\frac{(\omega_i - \overline{\omega})^2}{(\Delta\omega)^2}\right] \tag{22}$$

where $\overline{\omega}$ is the average transition frequency, $\Delta\omega = \gamma_{in\mathrm{hom}}(2\sqrt{\ln 2})^{-2}$, and γ_{inhom} is the inhomogeneous FWHM.

QD SOA can be used for the ultrafast and distortion-free amplification at pulse repetition rates of 20, 40, and 80 GHz with pulse durations of 710, 1.9, and 2.2 ps, respectively [9]. It should be noted that the amplification without patterning effect in QD SOA can be achieved at much lower pump current densities than in QW SOA [22].

4. Optical synchronization of a QDWELL laser dynamics and its influence on QDWELL laser and SOA performance

We investigated theoretically the optical synchronization of the carrier dynamics in the optically injected QDWELL laser and SOA and its influence on the QDWELL laser and SOA performance [23–27]. We solved numerically the LS equations (14)–(17) for the optically injected QDWELL laser [24–26] and Eqs. (17)–(22) for the QDWELL SOA [23, 27] using the typical values of QDWELL parameters and explicit expressions for the carrier scattering rates S_e^{in}, S_e^{out}, S_h^{in}, S_h^{out} [17, 20]. We used the MATLAB environment for the numerical simulations. We obtained a large number of the simulation results for the QW and QD carrier dynamics, QDWELL laser and SOA output signal eye diagrams, QD electron and hole phase trajectories, constellations for the QDWELL laser output 4-quadrature amplitude (4-QAM) modulation signal, QDWELL SOA gain wavelength and power dependence, QDWELL SOA chirp and extinction ratio (ER) dependence on the detuning between the pump and signal waves. They can be found in Refs. [23–27]. In this section, we summarize the main results and present the figures that demonstrate the influence of the optical injection on the QDWELL laser and QDWELL SOA performance.

It has been shown that the sufficiently strong optical injection leads to the synchronization of the electron and hole dynamics in QD [24]. In the transient turn-on regime, the bias current

and the optical output pulses are strongly synchronized in the case of a comparatively high optical injection power of several milliwatts and the moderate bias current density $j = 3j_{th}$, where $j_{th} \approx 6.7A/m^2$ is the threshold current density of the QDWELL laser [24]. In such a case, $\rho_e + \rho_h < 1$, and the term describing the inversion of the two-level system with electrons and holes is negative: $(\rho_e + \rho_h - 1) < 0$. It is seen from Eqs. (14)–(16) that the optically induced transitions in QD are dominant, and the QD electron and hole occupation probabilities ρ_e, ρ_h increase. Their increase is limited by the condition $\rho_e + \rho_h = 1$. Then, the first term in Eqs. (14)–(16) vanishes, and the QD carrier dynamics is determined by the spontaneous transition rate $R_{sp}(\rho_e, \rho_h)$ and essentially different carrier scattering rates S_e^{in}, S_e^{out}, S_h^{in}, S_h^{out} in and out of QD. The photons are mainly absorbed as it is shown in Eq. (14). In the case of a low level of optical injection less than 1 mW, large bias current density $j = 6j_{th}$ and a significant detuning $\Delta\nu_{inj} = 5GHz$ close to the RO frequency of 7 GHz electron occupation probability ρ_e strongly oscillates while the QD hole and QW carrier dynamics remains stable.

The large-signal response of the QDWELL laser is important for digital communication systems. In the case without the optical injection, the QDWELL laser large-signal dynamics is determined by the QW carrier densities w_e, w_h and their lifetime [17]. The sufficiently strong optical injection of the master laser is inserted instead of a large bias current provides a large enough QD carrier density [24]. In such a case, a device heating by the bias current does not occur. The radiative transition rates in QD are determined by the optical injection power and the frequency detuning $\Delta\nu_{inj}$ between the master and slave lasers [24]. The fast stimulated transitions in QD are dominant, and the increase of the optical injection power results in the stronger electron and hole dynamics synchronization. The QW carrier density is varying weakly. In the case of the electrical pseudorandom binary sequence (PRBS) input signal, the modulation frequency may be increased up to 30 GHz due to the enhanced RO frequency [24]. The boundaries of the stable OIL regime are determined by the following condition [28]

$$-K\frac{E_{inj}}{E_0}\sqrt{1+\alpha^2} \le 2\pi\Delta\nu_{inj} \le K\frac{E_{inj}}{E_0} \tag{23}$$

where E_0 and E_{inj} are the slave and master laser field amplitudes, respectively. The instability occurs and the QDWELL output signal manifests strong oscillations in the case of the large detuning, low bias current density $j = 2j_{th}$, and low optical injection level [25]. The eye diagrams of the QDWELL under strong optical injection power $P_{inj} > 1$mW start to deteriorate at the repetition frequency of 30 GHz [24, 25].

The directly modulated QDWELL laser can be introduced into an analogous optical link (AOL) in the framework of ultra wideband (UWB) radio-over-fiber (UROOF) technology [26, 29, 30]. The UWB high-speed AOL shown in **Figure 7** consists of electrical/optical (E/O) converter, a standard SMF (SSMF) optical fiber, and optical/electrical (O/E) converter [30]. We solved numerically Eqs. (14)–(19) for the AOL based on the optically injected QDWELL laser and standard SMF (SSMF) [26]. We considered the small UWB signal with the modulation frequency of 60 GHz, the zero detuning $\Delta\nu_{inj} = 0$ between the master laser and the QDWELL slave laser radiation, the 4-quadrature amplitude modulation (4-QAM) format, and

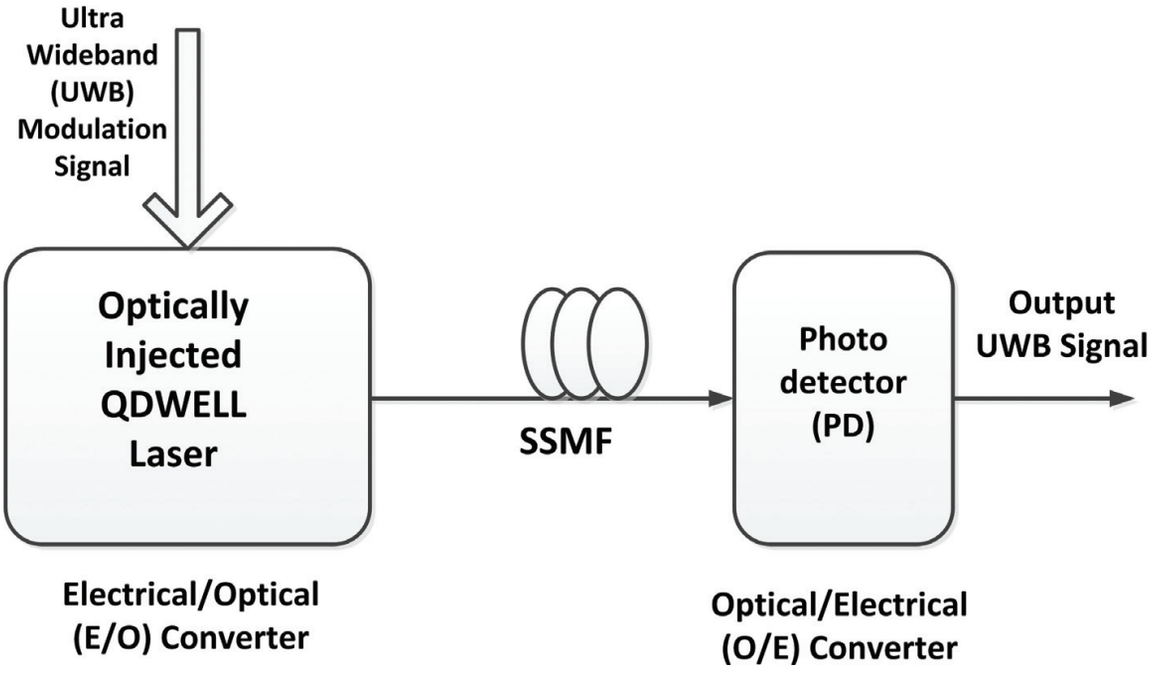

Figure 7. UWB analogous optical link (AOL) with the optically injected QDWELL laser (see **Figure 5**).

128 subcarriers with a 500 MHz bandwidth, and the direct bias current density j= $2j_{th}$. The dynamics of QD and QW carriers under the strong optical injection of about 1 mW is synchronized, which results in the improvement of the AOL performance.

The calculated constellation of the output 4-QAM modulation signal under the strong optical injection of about 1 mW is shown in **Figure 8**.

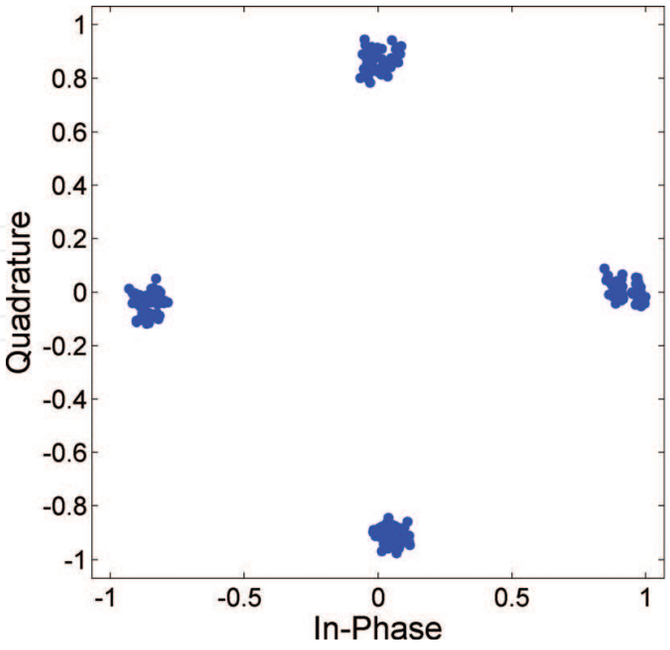

Figure 8. The calculated constellation of the output 4-QAM modulation signal for the modulation frequency 60 GHz, zero detuning, and the optical injection power of 1 mW.

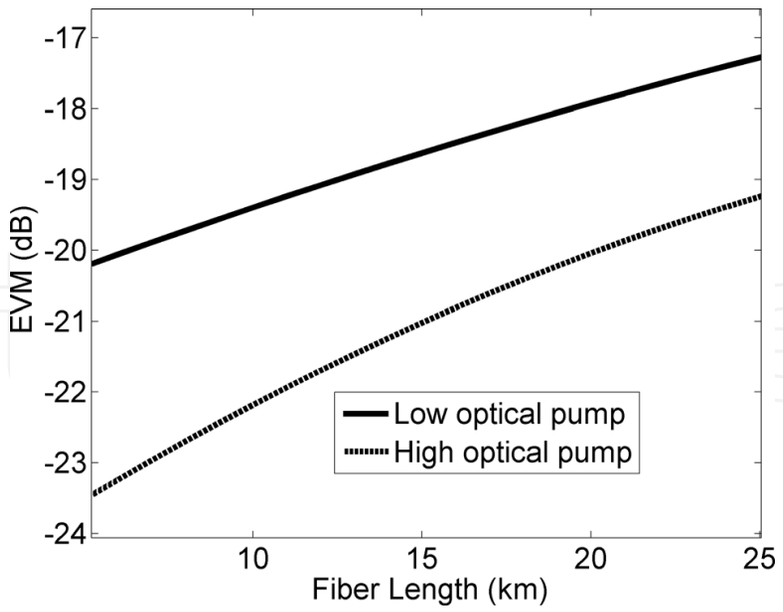

Figure 9. The calculated AOL EVM dependence on the distance for the low optical injection power of 10^{-3} mW (the upper curve) and for the high optical injection power of 1 mW (the lower curve).

The constellation shown in **Figure 8** is practically identical with the constellation of the input signal unlike the case without the optical injection [26]. The AOL error vector magnitude (EVM) dependence on the distance for the optical injection power of 10^{-3} and 1 mW is presented in **Figure 9**.

It is shown in **Figure 9** that in the case of the strong optical injection, the AOL EVM decreases significantly due to the enhancement of the QDWELL laser modulation frequency [26].

The spectrum of the detected UWB signal for the modulation frequency of 60 GHz, zero detuning between the master and the slave lasers, high optical injection power of 1 mW, and the propagation distance of 50 km is shown in **Figure 10** [26].

Consider now the influence of the optical pumping on the QDWELL SOA performance [23, 27]. We investigated the copropagating pumping and signal optical waves characterized by the optical power $P_{p,s}$ and the wavelengths $\lambda_{p,s}$, respectively [23]. Eqs. (17)–(22) have been solved numerically for the pulse regime and the large PRBS signal response [23]. The central pumping and signal wavelengths are $\lambda_p = 1.25$ μm and $\lambda_s = 1.35$ μm, respectively, and the optical pumping power is $P_p = 2,\ 5,\ 10$ mW [23]. The interaction of the pumping and signal wave in a QDWELL SOA results in the nonlinear optical phenomenon of the cross-gain modulation (XGM) [31]. During the XGM process, the strong modulated pumping wave imposes the modulation on the weak CW signal wave [31]. In such a case, SOA is acting as a wavelength converter (WC) transposing information at one wavelength to the signal at another wavelength [31]. In the case of a QDWELL SOA, the strong pumping wave at the same time synchronizes the QD and QW carrier dynamics. Indeed, when the pumping power $P_p = 1$ μW is small compared to the signal power $P_s = 1$ mW, the electron and hole dynamics in QD is desynchronized, the gain recovery time is determined by the carrier scattering rates

http://dx.doi.org/10.5772/intechopen.69946

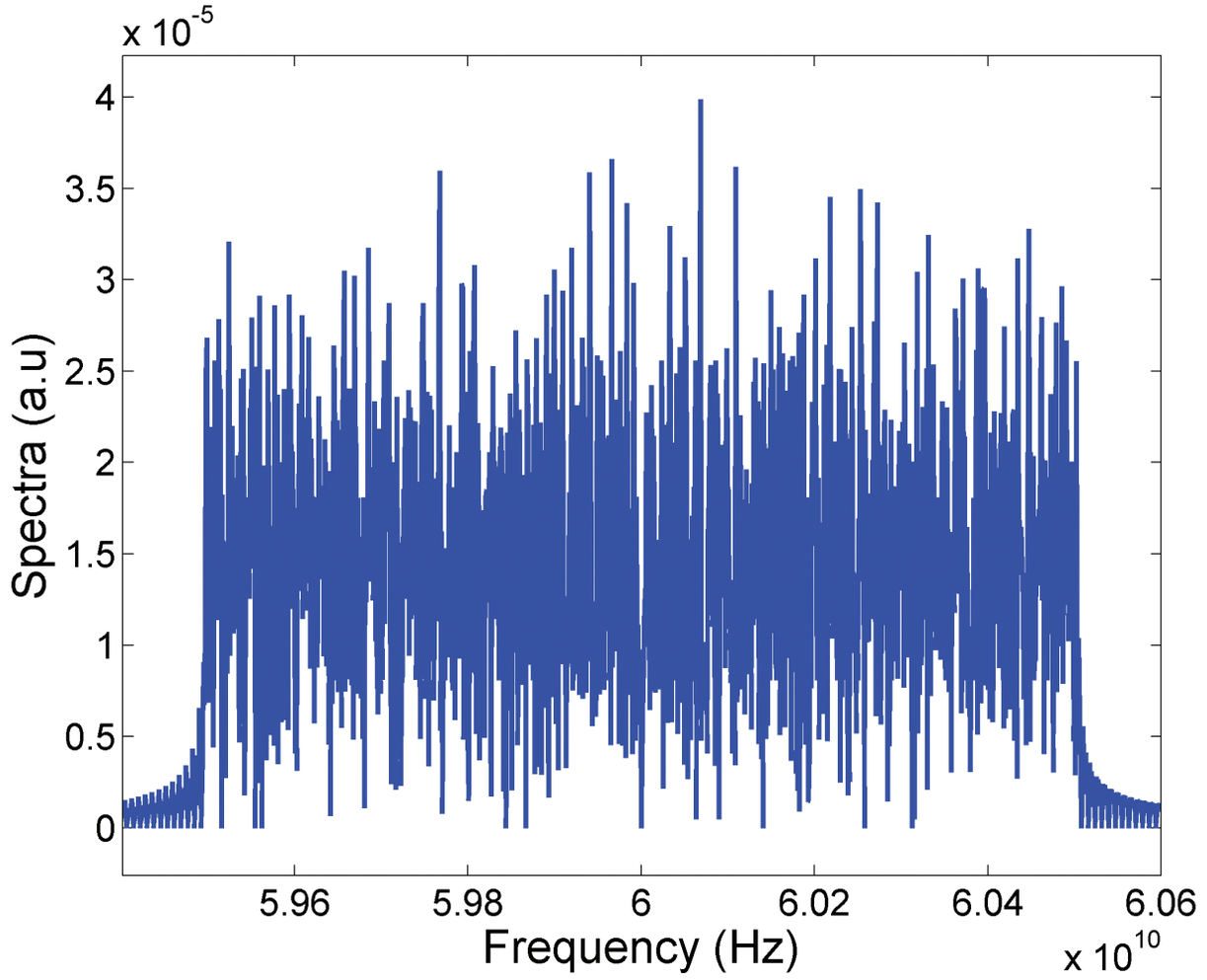

Figure 10. The calculated spectrum of the detected UWB signal after the propagation over the distance of 50 km for the modulation frequency of 60 GHz, zero detuning, and high optical injection power of 1 mW.

S_e^{in}, S_e^{out}, S_h^{in}, S_h^{out}, and the gain recovery process is slow [23]. In the opposite case of the strong pumping power of about 1 mW, the QD electron and hole dynamics is synchronized, the QD carrier occupation probabilities remain practically constant, and the gain recovery time decreases. The oscillation period of the QD carrier occupation probabilities ρ_e, ρ_h is determined by the optically enhanced gain recovery time [23]. The signal wave gain decreases with the increase of the pumping wave power due to XGM and the gain saturation at a large optical power. The bias current density influence on the gain is weak because of the weak connection between QW carrier reservoir and QD during the XGM process [23]. Under the strong optical of 1 mW and the low bias current density of $2j_{th}$, the QDWELL SOA performance improves. The eye diagram of the QDWELL SOA in such a regime is shown in **Figure 11**.

Figure 11 shows that the pattern effect in the eye diagram vanishes up to the repetition frequency of 140 Gb/s. The output signal optical power and chirp time dependence are shown in **Figure 12**. It is shown in **Figure 12** that due to the carrier dynamics synchronization provides the XGM process without the pattern effect, and the chirp reduces to about 5GHz and becomes symmetric [23, 27].

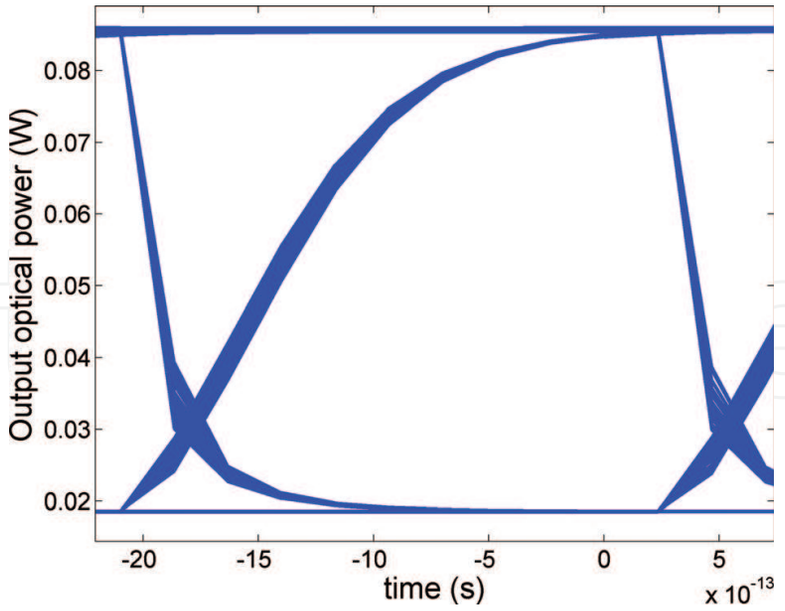

Figure 11. The output signal eye diagram for the signal power of 1 mW, optical pumping power of 2 mW, the bias current density of $2j_{th}$, and modulation bit rate of 140 GB/s.

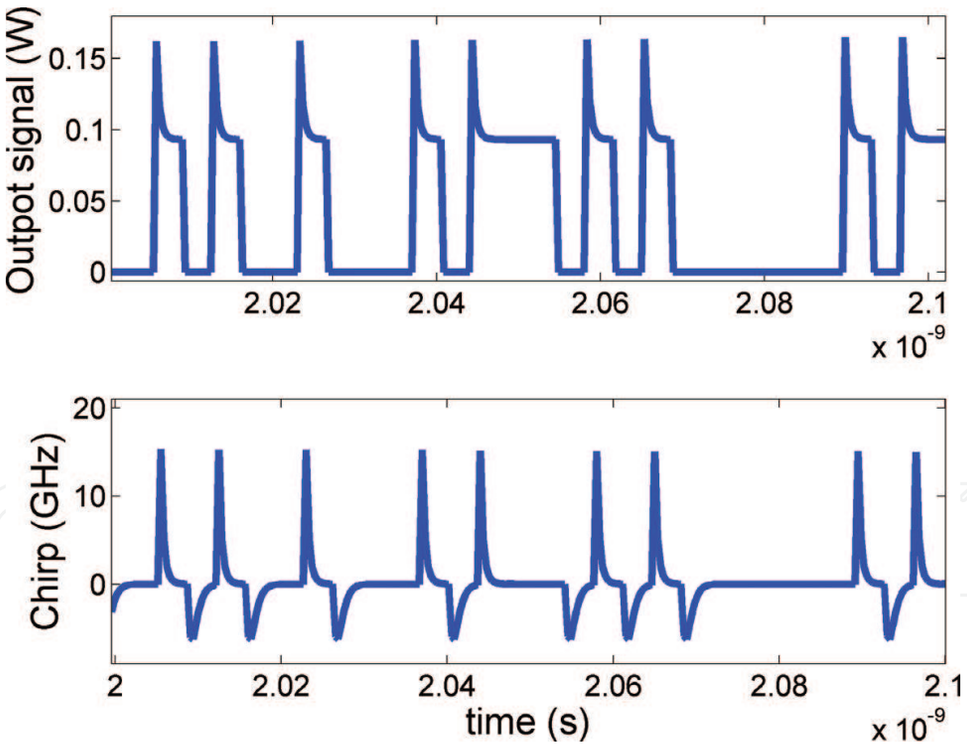

Figure 12. The optical power (the upper box) and the chirp (the lower box) of the output signal.

The strong optical pumping wave of several milliwatts during the XGM process may enhance the QDWELL SOA bandwidth up to 100 nm for a central wavelength of 1350 nm [27]. We investigated the ER dependence on the XGM detuning for the signal wave wavelength

http://dx.doi.org/10.5772/intechopen.69946

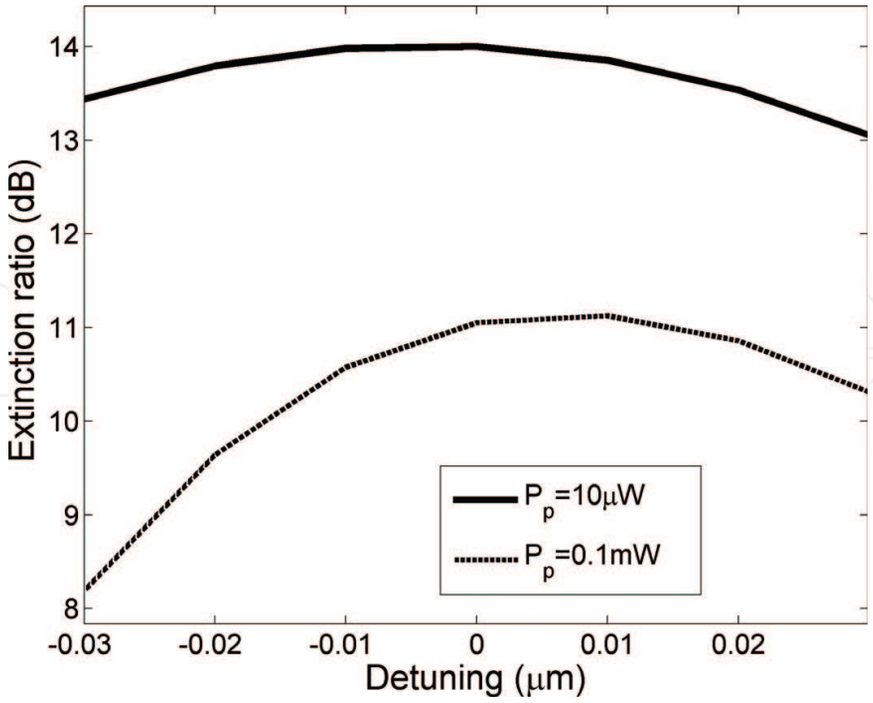

Figure 13. ER dependence on the XGM detuning for the signal wave wavelength $\lambda_s = 1.35$ μm, the signal wave optical power $P_s = 1$ mW, the bias current density of $2j_{th}$, and the CW pumping wave power P_p of 0.1 mW (the lower curve), 0.01 mW (the upper curve).

$\lambda_s = 1.35$μm and optical power $P_s = 1$ mW, and the CW pumping wave power P_p of 0.1 and 0.01 mW [27]. The simulation results are shown in **Figure 13**.

ER reduces with the increase of the CW pumping wave power P_p as it is shown in **Figure 13**.

5. Conclusions

QW and QD semiconductor lasers and SOA are promising candidates for applications in modern optical communication systems due to their comparatively low threshold current, high operation rate, high modulation bandwidth, low chirp, patterning-free operation, and stability with respect to temperature variations. These QW and QD advantages are mainly caused by the one-dimensional (1D) carrier localization in QW and three-dimensional carrier localization in QD. QDWELL lasers are based on the number of QW layers with the embedded QD. In such a case, 2D electron and hole gas also exists in a QW carrier reservoir, i.e., WL. QDWELL lasers are characterized by the lowest possible threshold current and fast QD carrier dynamics due to the 3D localization of electrons and holes in QD. However, the carrier dynamics in QW and QD is desynchronized due to the strong nonlinear carrier scattering rates for the electron and hole transitions in and out of QD. As a result, the modulation frequency of QDWELL lasers is limited by a comparatively low RO frequency of about 7 GHz. The modulation frequency can be enhanced by an increase of the injection current. But the increase of the injection current leads to the QDWELL laser heating and significant performance deterioration.

The modulation frequency and operation rate of semiconductor lasers and SOA can be improved by OIL using the master laser for the optical injection of the slave laser. We solved numerically the system of LS rate equations for QDWELL laser including the optical injection, the explicit expressions for the nonlinear carrier scattering rates, and the inhomogeneous spectral broadening specific for QD. The simulation results show that the carrier dynamics in QW and QD is synchronized by the sufficiently strong optical injection power $P_{inj} > 1$ mW since the fast stimulated transitions become dominant. As a result, the modulation frequency increases up to 30 GHz when the QDWELL output signal eye diagrams start to deteriorate. The high level of the carrier density in QD is provided by the optical injection, and the influence of the bias current is negligible. The strong bias current is not necessary, and the device heating and degradation are avoided. The optical injection process strongly depends on the frequency detuning between the master laser and the QDWELL slave laser. For the low optical injection power and the large detuning of about 10 GHz, the instability occurs accompanied by the strong oscillations of the QDWELL laser output signal. We solved the LS rate equations for AOL based on the optically injected QDWELL laser in the direct modulation regime for the optical injection power of 1 mW, zero detuning, 4-QAM modulation format, and 128 subcarriers with a 500 MHz bandwidth. In such a case, AOL manifests high performance up to the modulation frequency of 60 GHz.

TWA QDWELL LED with an input optical signal operates as a QDWELL SOA. QDWELL SOA is described by the modified system of rate equations including the equations for the pumping and signal wave photon densities. In such a case, the sufficiently strong pumping wave simultaneously plays a role of the optical injection and synchronizes the carrier dynamics in QW and QD. The nonlinear optical processes of XGM and XPM occur in a QDWELL SOA. QDWELL SOA performance is improved, the fast gain recovery takes place, the gain bandwidth is enhanced, ER and chirp decreases.

Author details

Yossef Ben Ezra[1,2] and Boris I. Lembrikov[1]*

*Address all correspondence to: borisle@hit.ac.il

1 Department of Electrical Engineering and Electronics, Holon Institute of Technology (HIT), Holon, Israel

2 MER Cellos, Holon, Israel

References

[1] Agrell E, Karlsson M, Chraplyvy AR, et al. Roadmap of optical communications. Journal of Optics. 2016;**18**(6):1-40. DOI: 10.1088/2040-8978/18/6/063002

[2] Agrawal GP. Fiber-optic Communication Systems. 4th ed. New York: Wiley; 2010. ISBN: 978-0-470-50511-3

[3] Agrawal GP. Nonlinear Fiber Optics. 5th ed. New York: Academic Press; 2013. ISBN: 978-0-12397-023-7

[4] Shieh W, Djordjevic I. Orthogonal Frequency Division Multiplexing for Optical Communications. London: Academic Press Elsevier; 2010. ISBN: 978-0-12-374879-9

[5] Ip E, Pak Tao Lau A, Barros DJF, Kahn JM. Coherent detection in optical fiber systems. Optics Express. 2008;**16**:753-791. ISSN: 1094-4087

[6] Zhao B, Yariv A. Quantum well semiconductor lasers. In: Kapon E, editor. Semiconductor Lasers I. Fundamentals. New York: Academic Press; 1999. pp. 1-121. ISBN: 0-12-397630-8

[7] Harrison P. Quantum Wells, Wires and Dots. Chichester, England: Wiley; 2005. p. 482. ISBN-13: 978-0-470-01079-2

[8] Nagarajan R, Bowers JE. High-Speed lasers. In: Kapon E, editor. Semiconductor Lasers I Fundamentals. New York: Academic Press; 1999. pp. 177-290. ISBN: 0-12-397630-8

[9] Rafailov EU, Cataluna MA, Avrutin EA. Ultrafast Lasers Based on Quantum Dot Structures. Weinheim: Wiley-VCH; 2011. p. 250. ISBN: 978-3-527-40928-0

[10] Lüdge K. Modeling Quantum-Dot-Based devices. In: Lüdge K, editor. Nonlinear Laser Dynamics. Weinheim, Germany: Wiley-VCH; 2012. pp. 1-33. ISBN: 978-0-470-85619-2

[11] Ustinov VM, Zhukov AE, Egorov AY, Maleev NA. Quantum Dot Lasers. Oxford: Oxford University Press; 2003. ISBN: 0 19 852679 2

[12] Ledentsov NN, Bimberg D, Alferov ZI. Progress in epitaxial growth and performance of quantum dot and quantum wire lasers. Journal of Lightwave Technology. 2008;**26**:1540-1555. DOI: 10.1109/JLT.2008.923645

[13] Coleman JJ, Young JD, Garg A. Semiconductor quantum dot lasers: A tutorial. Journal of Lightwave Technology. 2011;**29**:499-5102011. DOI: 10.1109/JLT.2010.2098849

[14] Malić E, Bormann MJP, Hövel P, Kuntz M, Bimberg D, Knorr A, Schöll E. Coulomb damped relaxation oscillations in semiconductor quantum dot lasers. IEEE Journal of Selected Topics in Quantum Electronics. 2007;**13**:1242-1247. DOI: 10.1109/JSTQE.2007.905148

[15] Lüdge K, Bormann MJP, Malić E, Hövel P, Kuntz M, Bimberg D, Knorr A, Schöll E. Turn-on dynamics and modulation response in semiconductor quantum dot lasers. Physical Review B. 2008;**78:**035316-1-035316-11. DOI: 10.103/PhysRevB.78.035316

[16] Lüdge K, Schöll E. Quantum-dot lasers—Desynchronized nonlinear dynamics of electrons and holes. IEEE Journal of Quantum Electronics. 2009;**45**:1396-1403. DOI: 10.1109/JQE.2009.2028159

[17] Lüdge K, Aust R, Fiol G, Stubenrauch M, Arsenijević D, Bimberg D, Schöll E. Large-signal response of semiconductor quantum-dot lasers. IEEE Journal of Quantum Electronics. 2010;**46**:1755-1762. DOI: 10.1109/JQE.2010.2066959

[18] Lüdge K, Schöll E. Nonlinear dynamics of doped semiconductor quantum dot lasers. The European Physics Journal D. 2010;**58**:167-174. DOI: 10.1140/epjd/e2010-00041-8

[19] Lau EK, Wong LJ, Wu MC. Enhanced modulation characteristics of injection-locked lasers: A tutorial. IEEE Journal of Selected Topics in Quantum Electronics. 2009;**15**:618-633. DOI: 10.1109/JSTQE.2009.2014779

[20] Pausch J, Otto C, Tylaite E, Majer N, Schöll E, Lüdge K. Optically injected quantum dot lasers: Impact of nonlinear carrier lifetimes on frequency-locking dynamics. New Journal of Physics. 2012;**14**:1-20. DOI: 10.1088/1367-2630/14/053018

[21] Agrawal GP, Olsson NA. Self-phase modulation and spectral broadening of optical pulses in semiconductor optical amplifiers. IEEE Journal of Quantum Electronics. 1989;**25**:2297-2306. DOI: 0018-9197/89/1100-2297

[22] Uskov AV, Berg TW, Mork J. Theory of pulse-train amplification without patterning effects in quantum-dot semiconductor optical amplifiers. IEEE Journal of Quantum Electronics. 2004;**40:**306-320. DOI: 10.1109/JQE.2003.82032

[23] Ben Ezra Y, Lembrikov BI. Semiconductor optical amplifier based on a quantum Dot-in-a-Well (QDWELL) structure under optical pumping. IEEE Journal of Quantum Electronics. 2014;**50**:340-347. DOI: 10.1109/JQE.20142308393

[24] Ben Ezra Y, Lembrikov BI. Synchronized carrier dynamics in quantum Dot-in-a-Well (QDWELL) laser under an optical injection. IEEE Journal of Selected Topics in Quantum Electronics. 2013;**19**:1-8. DOI: 10.1109/JSTQE.2013.2246770

[25] Ben Ezra Y, Lembrikov BI. Quantum Dot-in-a-Well (QDWELL) laser dynamics under optical injection. Optical and Quantum Electronics. 2014;**46**:1239-1245. DOI: 10.1007/s11082-013-9829-3

[26] Ben Ezra Y, Lembrikov BI. UWB system optical link based on a Quantum-Dot-in-a-Well (QDWELL) laser. Optical and Quantum Electronics. 2015;**47**:1527-1533. DOI: 10.1007/s11082-015-0154-x

[27] Ben Ezra Y, Lembrikov BI. Investigation of a cross-gain modulation (XGM) in a semiconductor optical amplifier (SOA) based on a quantum Dot-in-a-Well (QDWELL) structure. IET Optoelectronics. 2015;**9**:43-51. DOI: 10.1049/iet-opt.2014.0061

[28] Chang-Hasnain CJ, Zhao X. Ultrahigh-speed laser modulation by injection locking. In: Kaminov IP, Li T, Willner AE, editors. Optical Fiber Telecommunications. V A. Components and Subsystems. London: Elsevier Academic Press; 2008. pp. 145-182. ISBN: 978-0-12-374171-4

[29] Ran M., Ben Ezra Y., Lembrikov B. I. Ultra-wideband radio-over-optical fibre technologies. In: Kraemer R, Katz M., editors. Short-Range Wireless Communications: Emerging Technologies and Applications. Harvard: Wiley; 2009. pp. 271-327. ISBN: 978-0-470-69995-9

[30] Ran M, Ben Ezra Y, Lembrikov BI. High performance analog optical links based on quantum dot devices for UWB signal transmission. In: Lembrikov BI, editor. Ultra Wideband. Croatia: InTechOpen; 2010. pp. 75-96. ISBN: 978-953-307-139-8

[31] Connely MJ. Semiconductor Optical Amplifiers. London: Kluwer; 2002. p. 169. ISBN: 0-7923-7657-9

IntechOpen

IntechOpen